Growth Mechanism of Single-Walled Carbon Nanotube from Catalytic Reaction Inside Carbon Nanotube Template

Yoshifumi Izu,[†] Junichiro Shiomi,[†,*] Yoshiteru Takagi,[‡,§] Susumu Okada,[‡,§] and Shigeo Maruyama[†,*]

[†]Department of Mechanical Engineering, The University of Tokyo, Tokyo 113-8656, Japan, [‡]Institute of Physics and Center for Computational Sciences, University of Tsukuba, 1-1-1 Tennodai, Tsukuba 305-8577, Japan, and [§]Japan Science and Technology Agency, CREST, 5 Sanbancho, Chiyoda-ku, Tokyo 102-0075, Japan

ABSTRACT We report a numerical investigation on the catalytic growth mechanism of a single-walled carbon nanotube (SWNT) inside a template SWNT, that is, formation of a double-walled carbon nanotube (DWNT). The molecular dynamics simulations together with complementary ab inito calculations suggest that the DWNT formation from thermally annealed metallocene-encapsulating SWNT goes through formation of metal catalyst cluster, followed by SWNT precipitation at the root. The diameter of the inner SWNT is determined by the carbon/metal layered structure of the catalyst cluster, which gives rise to a DWNT interlayer distance significantly different from the van der Waals distance.

KEYWORDS: carbon nanotube · growth mechanism · metallocene · encapsulation · molecular dynamics · density function theory

Carbon nanotubes (CNTs) have been celebrated for their novel electrical, optical, thermal, and mechanical properties arising from the quasi-one-dimensional structure with seamless covalent bond networks.[1] One direct application of the unique geometry, among many, is the nanoscale reactor to realize chemical reactions in the quasi-one-dimensional interior. Such chemical reactors are promising platforms for invention of new materials with restricted structures and low dimensional properties.[2−9] Interiors of CNTs also offer chemically and thermally stable environments for subtle chemical reactions. In addition, high reaction efficiency can be achieved by the directional molecular diffusion and high molecular collision rate under the confinement. Furthermore, CNTs serve as an ideal support for single molecule observation under transmission electron microscope.[10] With this multifunctional feature, CNT could be thought as a "nanoscale laboratory", a foundation for future nanomaterial innovations.

A successful demonstration of the above concept can be found in formation of a CNT inside a template CNT.[2−7] An ultimate case is when the CNTs are single-walled carbon nanotubes (SWNTs), which results in a formation of a double-walled carbon nanotube (DWNT). It has been well-known that DWNTs can be formed by thermalizing peapods (SWNTs filled with fullerenes).[2−4] More recently, it was shown that DWNTs can also be synthesized by thermally annealing SWNTs encapsulating ferrocene.[5,7,8] A key finding in these works is that the diameter of the inner SWNT depends on the synthesis method. Shiozawa *et al.*[8] showed by using detailed resonant Raman spectroscopy that DWNTs formed from the ferrocene-encapsulating SWNTs exhibit considerably larger interlayer distance (*i.e.*, smaller inner tube diameter for the same outer tube) than that from peapods. The finding opens up a possibility for tailoring the interlayer distance and thus the properties of DWNTs, complementing other well-explored growth methods such as the arc discharge[11−13] and chemical vapor deposition.[14−17] This is impacting since DWNTs are expected to possess similar low dimensional transport properties as SWNTs with even better mechanical strength, and hence, are attractive building blocks for various nanodevices. Furthermore, recent experiments have probed the dependence of the charge transfer on annealing temperature and kind of metallocene, which suggests the possibility for tuning of the electrical properties of nanotubes by filling with metallocene and annealing.[18,19] However, the cause of the different interlayer distances is not understood yet, and it is of a primary task to identify the growth mechanism of the inner SWNT inside the nanotube templates.

*Address correspondence to shiomi@photon.t.u-tokyo.ac.jp, maruyama@photon.t.u-tokyo.ac.jp.

Received for review March 7, 2010 and accepted July 01, 2010.

Published online July 13, 2010. 10.1021/nn100461r

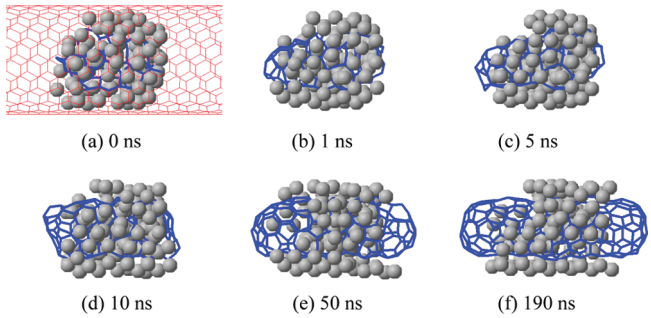

Figure 1. Growth process of an SWNT (blue) inside a template (10, 10) SWNT (red). Covalent bonds of the inner and outer SWNTs are denoted with blue and red lines. The outer SWNT is omitted in images b−f for visual clarity.

The DWNT formation from thermally annealed peapods can be pictured as fullerenes fusing and relaxing into an SWNT. The experiments have shown that the interlayer distance differs from the typical van der Waals distance of graphite and multiwalled CNT, though the sign of the difference depends on the report.[4,8] Nevertheless, the interlayer distance is expected to depend on the kinetic path of the polymerization of fullerene precursors as shown by the molecular dynamics simulations.[20,21] On the other hand, the understanding of the formation process of DWNTs from metallocene-encapsulating CNTs is much more limited. Although the experiments have probed signatures of catalytic growth from metal carbide clusters,[8] no temporally resolved microscopic analysis is available to this date. Therefore, in this work, we study the growth process of an inner SWNTs from catalytic reaction inside a template SWNT by using molecular dynamics (MD) simulations. By choosing nickel as the representative transition metal, the catalytic reaction of the feedstock carbon atoms and metal carbide inside a template SWNT was modeled by adopting the set of potential functions that has been successful in simulating the nucleation of metallofullerenes[22] and SWNTs[23] from floating catalysts. On the basis of the general growth mechanism obtained from the MD simulations, we further quantify the interlayer distances of the DWNT by using an *ab initio* calculation, which allows us to compare the numerical simulations with the experiments and to validate the growth model.

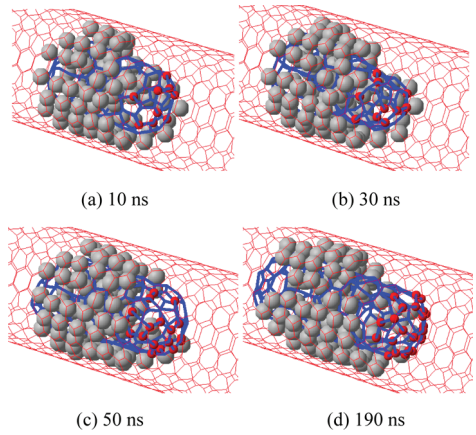

Figure 2. Trajectories of carbon atoms. The carbon atoms forming the cap at $t = 190$ ns are denoted with red spheres.

RESULTS AND DISCUSSION

The trajectories obtained from the MD simulations clearly show the growth of the inner SWNT from the catalyst cluster. Figure 1 depicts a case simulated until $t = 190$ ns, starting from an initial condition with Ni_{97} carbide cluster encapsulated in a (10, 10) SWNT. At the early stage, the feedstock carbon atoms cover the cluster surface except for the part in contact with the outer SWNT. Once all the open sites are occupied, the carbon atoms precipitate to form a cap structure and then an SWNT. The general trend was the same for other cases with different outer SWNT chiralities and initial cluster sizes. To gain insight into the dynamics of the cluster during the SWNT growth, the Lindemann index[24] of the carbon atoms in the cluster was calculated. As a result, the index was found to always remain well below 0.1 (Supporting Information, Table S1), the threshold value below which the system can be considered to be solid.[25] This indicates that the carbon structure inside the metal carbide cluster is stable and additional carbon atoms from the feedstock hardly diffuse into the cluster throughout the growth process.

More details of the carbon supply process was studied by marking (with red spheres) the carbon atoms that formed the tip of the cap at $t = 190$ ns and monitoring their trajectories during the growth process (Figure 2). The visualized trajectories reveal that the feedstock carbon atoms mainly adsorb onto the open sites of the outermost metal layer of the cluster and then are carried away from the cluster as more carbon atoms are fed and precipitate. This suggests the growth mechanism shown in Figure 3 for the catalytic reaction inside a template SWNT; once the cap is formed, carbon atoms are fed from the root of the cap to realize continuous growth of the inner SWNT.

The growth simulations for template SWNTs with various chiralities reveal the influence of the template geometry on the resulting structure of the inner SWNT. A general and most important characteristic is that the inner SWNT diameter is well-correlated with the outer SWNT diameter keeping the interlayer distance at a constant value, which will be discussed later. For now, let us briefly discuss the structural details, if the chiral angle has noticeable influence on the structure of the inner SWNT. To investigate the influence of the chiral

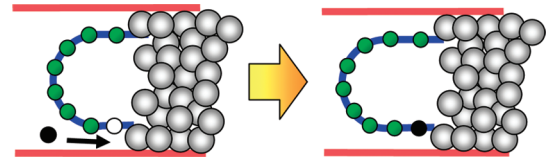

Figure 3. Schematics of inner SWNT growth process.

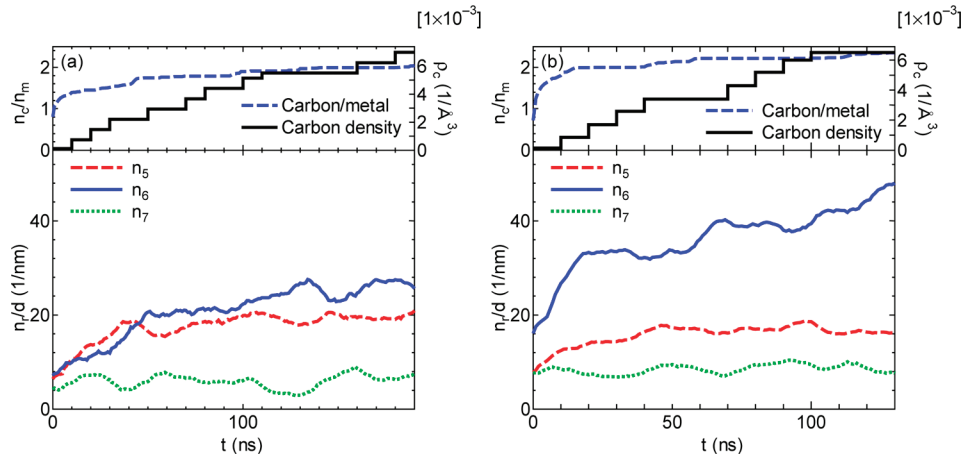

Figure 4. Structural properties of the inner SWNT growth for (a) (10, 10) and (b) (15, 6) outer SWNTs. In the bottom figures, the time histories of the number of five-, six-, and seven-membered rings (n_5, n_6, n_7) are denoted with dashed, solid, and dotted lines, respectively. Here, d is the diameter of the outer SWNT, where $d = 1.38$ and 1.49 nm for (10, 10) and (15, 6) SWNTs, respectively. The top figure denotes the ratio of number of carbon atoms (n_c) to that of metal atoms (n_m) in the metal carbide cluster with the dotted lines, and the feedstock carbon density (ρ_c) with the solid lines.

angle of the template SWNT, simulations were performed for template SWNTs with different chiralities with similar diameters; (11, 11) and (15, 6). The result shows that the outermost nickel layer is aligned with the outer SWNT structure, with the nickel atoms locating near the hollow site of the graphitic network of the outer SWNT (Supporting Information, Figure S2). However, we could not observe a clear evidence of the metal alignment affecting the carbon structure precipitated from the catalyst cluster. Therefore the current simulations do not suggest selective influences of the outer SWNT chirality on the inner SWNT structure, although the presence of defects and lack of inner SWNT length prevent us from drawing a conclusion. The dependence on the cluster size was also investigated by varying the number of nickel atoms in the metal carbide cluster as 108, 128, and 158, which showed no deterministic influence on the resulting inner SWNT.

One useful way to characterize the formation of SWNT is to measure the number of five- to seven-membered rings.[23] This also allows us to monitor the time evolution of the growth process, that is, the growth rate. Figure 4a,b shows time histories of the number ratio of carbon to metal in the catalyst cluster (n_c/n_m), the number density of the feedstock carbon atoms (ρ_c), and the number of five- to seven-membered rings (n_5, n_6, n_7), for outer SWNTs with chiralities (10, 10) and (15, 6). Note that, to achieve monotonic growth, the number density of the feedstock carbon was increased with time. Although the time histories of ρ_c are not the same for the two cases reflecting the different growth rate, the difference is minor and should not affect the following discussions. For both cases, the n_6 profiles exhibit two regimes; an initial faster growth and the following slower growth, despite the gradual increase in the feedstock density. An insight into this can be gained from the n_5 profiles, which increase in the beginning and gradually saturate before $t = 50$ ns at a constant value. This corresponds to the formation of the cap structure which needs five-membered rings to form the 3-d curvature. Once the cap is formed, n_5 saturates at around a value of n_5/d ($=20$ nm^{-1}) independent of the outer SWNT diameter (d). Therefore, the above behavior of the n_6 profiles corresponds to the relatively fast nucleation of the cap and the slow growth of the side walls.

This agrees with the pictures shown in Figure 1, where the cap formation is completed before $t = 50$ ns. The growth deceleration can be understood from the growth mechanism described in Figure 3, where the feedstock needs to overcome the potential barrier to diffuse through the channel between inner and outer SWNTs, which becomes larger as the cap forms and the side wall grows. This also results in a much slower growth speed compared with the SWNT nucleation from the floating catalyst cluster in the previous molecular dynamics study.[23] While the general trend of the growth curves was the same for the two cases, the distinct difference in the magnitude of n_5/d suggests that the growth rate of the inner SWNTs sensitively depends on the outer diameter. Note that the magnitude of n_7 indicates the extent of defects, which is similar and relatively low in both cases.

Let us now investigate the interlayer distance of the DWNT. Taking the cases where highly crystallized DWNT growth was observed, the density distribution function (DDF) of the carbon atoms of the inner SWNT was calculated as a function of the radial distance from the outer SWNT (Figure 5). The interlayer distance was about 3.2 Å independently of the outer SWNT diameter, which is significantly different from the van der Waals distance (3.4 Å). The cause of the interlayer deviation can be understood by comparing the carbon DDFs of the inner SWNT and the catalyst cluster. The good match between the peak positions indicates that the diameter of the inner SWNT is determined by the carbon

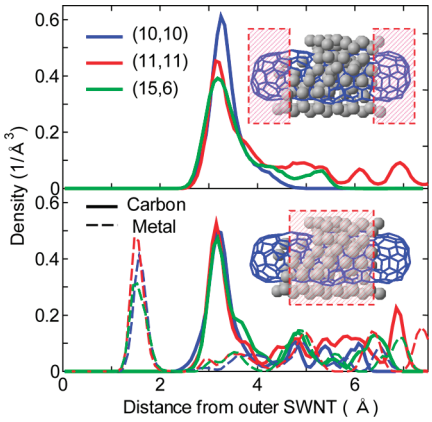

Figure 5. Density distribution function of carbon/metal atoms in (top) the precipitated SWNT and (bottom) the metal carbide cluster, for three different outer SWNT chiralities.

structures inside the catalyst cluster. The primary role of the metal carbide structure over the interlayer van der Waals interaction was also checked by performing the simulations for two different models with and without van der Waals interactions between the inner and outer SWNTs (Supporting Information, Figure S3). Figure 5 also shows that the largest metal DDF peak is located right in between the largest carbon DDF peak and the outer SWNT, therefore the metal carbide cluster takes a distinct layered structure with outer metal and inner carbon layers. The DDFs together with molecular trajectory show that the outer layers of the cluster have an ordered structure by adopting the structure of the outer SWNT while the core of the cluster remains disordered. The above adds up to the following mechanism; equilibration of metal carbide cluster inside a template SWNT gives rise to a layered structure, where a metal layer is sandwiched between the template SWNT and the internal carbon layer. This structure guides the inner SWNT to grow preserving the interlayer distance between the carbon structure and the outer SWNT. Since the inner SWNT grows from the root, the structure is strongly influenced by the metal carbide structure at the SWNT/cluster interface, and thus inherits the diameter of the carbon layer in the catalyst cluster.

The MD simulations so far suggest that the diameter of the inner SWNT grown from the catalyst cluster inside a template SWNT is determined by the distance between the concentric carbon layers separated by the metal layer in between. This means that the inner SWNT diameter can be predicted by knowing the bond length of the intercalating structure. Then the next step is to check if this mechanism agrees with the available experiments. Since the quantitative comparison with the experiments on such a structure requires charge transfer effects, which cannot be taken into account in the current MD potential model, we have separately performed *ab initio* calculations based on the density functional theory (DFT).[26] For this, we have reduced the system to a metal atom intercalating two graphitic layers. Furthermore, by ignoring the curvature of SWNT for simplicity, the system can be considered as the conventional graphite intercalation compound (GIC). Iron (Fe) was chosen as the metal to compare the results with those of the experiment of DWNT formation by thermally annealing ferrocene encapsulating SWNTs.[8] For the DFT calculation, the generalized gradient approximation (GGA)[27] was adopted for the electron exchange-correlation potential, and electron−ion interaction was expressed using the ultrasoft pseudopotential. The valence electron wave functions were expanded using a plane wave basis with a kinetic cutoff energy of 36 Ry. The *ab initio* calculations of the Fe−GIC system with stable structure resulted in interlayer distance of 3.53 Å, which agrees well with the experiment.[8] The agreement supports the validity of the above growth mechanism obtained from the MD simulations; the inner SWNT grows through formation of the metal cluster and the interlayer distance is determined by the layered structure of the heterogeneous catalyst cluster.

The above molecular simulations assumed that the inner SWNT is grown from a metal cluster, based on the reported experimental observation.[8] However, especially at high temperature, the thermally decomposed species may start reacting and nucleating before forming a stable metal cluster. To validate this possibility and also to seek an alternative reaction pathway, we have performed additional simulations in the other extreme case: SWNT growth from catalytic reaction of fully thermally decomposed precursors. For the sake of simplicity and practicability in the molecular dynamics framework, we rephrase this as "catalytic reaction starting from individual carbon and metal atoms randomly placed inside a template SWNT". This was done using the same MD model as the previous simulation for a cluster, except for a modification on the metal−metal and metal−carbon binding energies. On beginning the simulation from initial conditions with isolated metal atoms, the surface diffusion length of the metal atoms on the template SWNT and the grown inner SWNT becomes considerably larger than that of the previous initial conduction with a cluster, and hence, plays an important role on determining the resulting inner SWNT growth. Therefore, the magnitude of the binding energy in the graphitic/metal layering structure becomes important even for qualitative characterization, unlike the previous simulation with minute diffusion of the cluster. For these reasons, we have incorporated the metal−graphite binding energy obtained from the above DFT calculation of the Fe−GIC system. As a result, the metal−carbon binding energy is approximately half of the value in the previous simulations for nickel carbide system. Correspondingly, the metal−metal binding energy was scaled by half to maintain the consistency.

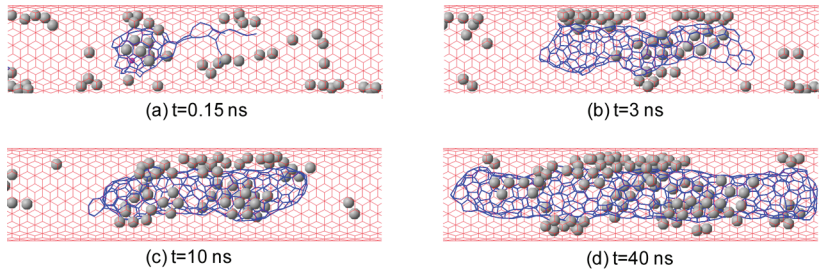

Figure 6. Growth process of an SWNT inside a (11, 11) SWNT from randomly placed individual carbon and metal atoms. Covalent bonds of the inner and outer SWNTs are denoted with blue and red lines.

The simulation begins by gradually feeding metal and carbon atoms inside the template SWNT with a number ratio of initially 1:2 and then 1:10 corresponding to that of metallocene. The temperature was kept the same as the previous simulations (2500 K). The number density of the carbon gas was kept constant. Note that carbon atoms are allowed to react only through catalyst metal atoms. As a consequence, this model realized highly efficient growth of the inner SWNT as seen in Figure 6, which shows the growth process inside a (11, 11) template SWNT until $t = 40$ ns. The figure clearly shows the initial formation of a patch of graphitic network (Figure 6a) and then a cap structure (Figure 6b,c) due to the catalytic activity of the metal in the form of a small cluster with several atoms. The metal particles are adsorbed onto the outer SWNT and act as a reaction site to further growth of inner SWNTs. The individual metal atoms or small cluster here exhibit longer diffusion lengths and are more volatile than the previous case with a nanoscale metal cluster. Therefore, in this case, the growth site is not fixed, but varies with time. The same growth process was observed for other kinds of outer SWNT chiralities. To the authors' knowledge, among many reported molecular dynamics simulations with non-*ad-hoc* and *ad hoc* MD models, the SWNT grown in the current simulation is one of the longest ones.

As in the previous case for growth from catalyst cluster, the density distribution function was calculated (Supporting Information, Figure S4), and the interlayer distance was obtained to be 3.4 Å corresponding with the van der Waals distance, independently of the outer SWNT diameter. This is because there are less metal particles around the growth site due to the relatively large growth site and high mobility of the metal atoms. Therefore, the results do not agree with the DWNT growth experiment from ferrocene encapsulating SWNTs,[8] and rather supports, though does not prove, the validity of the previous catalyst cluster model. On the other hand, it suggests there may be other possible growth paths that might be more efficient than the growth from the catalytic cluster.

SUMMARY AND CONCLUSIONS

The formation process of DWNTs from metallocene-encapsulating SWNTs was investigated by combining MD simulations and DFT calculations. First, by assuming the formation of catalyst nanocluster prior to the growth of inner SWNTs, the growth process was clearly identified by the MD simulations. The detailed observation of the molecular trajectories reveals the root growth of the inner SWNTs. Here, the carbon atoms access the catalyst through the potential barrier between the inner and outer SWNTs, which increases as the inner SWNT grows, and thus slows down the growth for constant feedstock density. The DDF of constituent atoms reveals that the DWNT interlayer distance significantly differs from the van der Waals distance for graphite and multiwalled CNTs. The good correlation between the DDFs of the precipitated SWNT and the layered metal carbide cluster suggests that the interlayer distance is determined by the carbon/metal layered structure of the metal carbide cluster. On the basis of the general mechanism obtained from the molecular dynamics simulations, the interlayer distance of the layered structure was quantified by performing *ab initio* calculations for Fe−GIC system. By taking iron as the metal, good agreement was obtained with the experiments on DWNT formation from ferrocene encapsulating SWNT. Further insight into the validity of the catalyst cluster model is gained by examining the other extreme growth scenario: growth of inner SWNTs from randomly placed individual carbon and metal atoms. This resulted in highly efficient growth, where the interlayer distance was equal to the van der Waals distance. Although this may suggest a possibility for more efficient pathways, the good agreement between the catalyst cluster model with the experiments suggests that the DWNT formation from ferrocene-encapsulating SWNTs goes through a formation of metal cluster.

METHODS

Growth Simulations. In the MD simulations, catalytic growth was simulated by feeding a carbon source to a stable metal cluster inside a template SWNT. The model assumes the formation of a stable metal carbide cluster prior to the SWNT growth. The model is further simplified by expressing the catalytic reaction between the metal cluster and the carbon source with the reaction of the cluster and individual carbon atoms (feedstock carbon atoms). In this model system, feedstock consists of indi-

vidual carbon atoms despite that it is metallocene in reality since molecular dynamics simulations including the decomposition process of metallocene would require a simulation time far beyond our computational resource. With this simplification, the model system assumes a scenario that the precursors are thermally decomposed prior to the formation of catalyst cluster and growth of inner nanotube.

For sake of computational time, the simulations were given quasi-deterministic initial conditions based on the knowledge learned from the previous simulations on SWNT growth from floating catalysts.[23] The previous work found that the efficiency of the cap nucleation depends on the contents of the graphitic network embedded in the metal carbide cluster. Therefore, in this study, we have tailored the initial nickel carbide cluster with high content of graphene networks (see Supporting Information for the methodology).

The growth simulations were performed for template SWNTs with various chiralities and metal carbide clusters with various sizes. The temperature was set at 2500 K, much higher than in the actual experiments,[8] in order to accelerate the simulation and also by considering the relatively high equilibrium binding energies of the current potential functions. The feedstock carbon atoms were fed at random locations inside the template SWNT by keeping the density of the isolated carbon atoms constant, that is, a new carbon atom was added for every carbon atom adsorbed onto the metal carbide cluster. An exception was made when no absorption took place for 10 ns, then the density was increased to speed up the process. The feedstock carbon atoms were not allowed to react with each other before they reached the metal carbide cluster. During the growth simulation, the 3-D periodic boundary conditions were adopted and the carbon atoms of the template SWNT were fixed at the equilibrium positions (adiabatic condition). All of the above simplifications were adopted in the MD model in order to simulate the entire process from nucleation to growth of inner SWNTs. While the literature offers various molecular dynamics approach with different levels of accuracy and concepts,[28−34] they all required a compromise between the simulation time and the model accuracy. Our strategy here is to identify a qualitative growth mechanism using simple classical molecular dynamics simulation and complement it with the *ab initio* calculation when quantification is necessary.

Molecular Dynamics Model. In the molecular dynamics model, the conventional Brenner potential[35] is used for the carbon covalent-bond interactions. Similarly, the metal−metal and metal−carbon interaction was modeled by the bond order potential developed by Yamaguchi and Maruyama.[22] The metal−carbon potential takes a form of multibody potential functions as a function of the carbon coordinate number of a metal atom. The binding energy is expressed as

$$E_b = V_R - V_A \tag{1}$$

$$V_R = f(r_{ij})\frac{D_e}{S-1}\exp\{-\beta\sqrt{2S}(r_{ij}-R_e)\} \tag{2}$$

$$V_A = f(r_{ij})B^*\frac{D_e S}{S-1}\exp\{-\beta\sqrt{2/S}(r_{ij}-R_e)\} \tag{3}$$

Here r_{ij} denotes the distance between ith metal and jth carbon. The bond order term B^* is expressed as a function of the coordinate number N^C defined in terms of the cutoff function $f(r)$,

$$B^* = \{1 + b(N^C - 1)\} \tag{4}$$

$$N^C = 1 + \sum_{\text{carbon } k(\neq j)} f(r_{ik}) \tag{5}$$

$$f(r) = \begin{cases} 1 & (r < R_1) \\ \frac{1}{2}\left(1 + \cos\frac{r-R_1}{R_2-R_1}\right)\pi & (R_1 < r < R_2) \\ 0 & (r > R_2) \end{cases} \tag{6}$$

The potential parameters were determined by fitting the above many-body potential function to a DFT calculation for MC_n clusters ($n = 1-3$).

The potential function for metal−metal interaction takes the same form as the metal−carbon interaction. Here, instead of adopting B^*, the equilibrium binding energy D_e and bond length were expressed as functions of the metal coordinate number (*i.e.* $B^* = 1$).

$$D_e(N_{ij}^M) = D_{e1} + D_{e2}\exp\{-C_D(N_{ij}^M - 1)\} \tag{7}$$

$$R_e(N_{ij}^M) = R_{e1} - R_{e2}\exp\{-C_R(N_{ij}^M - 1)\} \tag{8}$$

$$N_{ij}^M = \frac{N_i^M + N_j^M}{2}, \qquad N_i^M = 1 + \sum_{\text{metal } k(\neq j)} f(r_{ik}) \tag{9}$$

The potential parameters are presented in ref 22.

The equation of motion was numerically integrated using the velocity Verlet method with a time step of 0.5 fs. For the temperature control, the translational, rotational, and vibrational temperatures were independently controlled using the Brendsen method[36] with a relation time of 0.17 ps.

The interactions between the isolated carbon atoms were expressed by Lennard-Jones potential ($\varepsilon = 2.4$ meV, $\sigma = 3.37$ Å) to avoid the reaction between isolated carbon atoms. The same Lennard-Jones potential was also used to model the van der Waals interaction between the outer nanotube layer and the carbon atoms of the inner nanotube.

Acknowledgment. This work is supported in part by Grants-in-Aid for Scientific Research 19051016 and 19054003.

Supporting Information Available: Method of tailoring initial metal carbide cluster, data of Lindemann index calculations, and more details on outer-tube chirality dependence and density distribution functions. This material is available free of charge *via* the Internet at http://pubs.acs.org.

REFERENCES AND NOTES

1. *Carbon Nanotubes: Advanced Topics in the Synthesis, S., Properties and Applications*; Jorio, A., Dresselhaus, M. S., Dresselhaus, G., Eds.; Springer: Berlin, Heidelberg, and New York, 2008.
2. Smith, B. W.; Monthioux, M.; Luzzi, D. E. Encapsulated C60 in Carbon Nanotubes. *Nature* **1998**, *396*, 323–324.
3. Smith, B. W.; Luzzi, D. E. Formation Mechanism of Fullerene Peapods and Coaxial Tubes: A Path to Large Scale Synthesis. *Chem. Phys. Lett.* **2000**, *321*, 169–174.
4. Bandow, S.; Takizawa, M.; Hirahara, K.; Yudasaka, M.; Iijima, S. Raman Scattering Study of Double-Walled Carbon Nanotubes Derived From the Chains of Fullerenes in Single-Walled Carbon Nanotubes. *Chem. Phys. Lett.* **2001**, *337*, 48–54.
5. Guan, L.; Shi, Z.; Li, M.; Gu, Z. Ferrocene-Filled Single-Walled Carbon Nanotubes. *Carbon* **2005**, *43*, 2780–2785.
6. Rodriguez-Manzo, J. A.; Terrones, M.; Terrones, H.; Kroto, H. W.; Sun, L.; Banhart, F. *In Situ* Nucleation of Carbon Nanotubes by the Injection of Carbon Atoms into Metal Particles. *Nat. Nanotechnol.* **2007**, *2*, 307–311.
7. Pfeiffer, R.; Peterlik, H.; Kuzmany, H.; Shiozawa, H.; Grüneis, A.; Pichler, T.; Kataura, H. Growth Mechanisms of Inner-Shell Tubes in Double-Wall Carbon Nanotubes. *Phys. Stat. Sol. (b)* **2007**, *244*, 4097–4101.
8. Shiozawa, H.; Pichler, T.; Grüneis, A.; Pfeiffer, R.; Kuzmany, H.; Liu, Z.; Suenaga, K.; Kataura, H. A Catalytic Reaction Inside a Single-Walled Carbon Nanotube. *Adv. Mater.* **2008**, *20*, 1443–1449.
9. Kitaura, R.; Imazu, N.; Kobayashi, K.; Shinohara, H. Fabrication of Metal Nanowires in Carbon Nanotubes *via* Versatile Nano-Template Reaction. *Nano Lett.* **2008**, *8*, 693–699.
10. Koshino, M.; Tanaka, T.; Solin, N.; Suenaga, K.; Isobe, H.; Nakamura, E. Imaging of Single Organic Molecules in Motion. *Science* **2007**, *11*, 853.

11. Hutchison, J. L.; Kiselev, N. A.; Krinichnaya, E. P.; Krestinin, A. V.; Loutfy, R. O.; Morawsky, A. P.; Muradyan, V. E.; Obraztsova, E. D.; Sloan, J.; Terekhov, S. V.; Zakharov, D. N. Double-Walled Carbon Nanotubes Fabricated by a Hydrogen Arc Discharge Method. *Carbon* **2001**, *39*, 761–770.
12. Saito, Y.; Nakahira, T.; Uemura, S. Growth Conditions of Double-Walled Carbon Nanotubes in Arc Discharge. *J. Phys. Chem. B* **2003**, *107*, 931–934.
13. Sugai, T.; Yoshida, H.; Shimada, T.; Okazaki, T.; Shinohara, H. New Synthesis of High-Quality Double-Walled Carbon Nanotubes by High-Temperature Pulsed Arc Discharge. *Nano Lett.* **2003**, *3*, 769–773.
14. Bacsa, R. R.; Laurent, Ch.; Peigney, A.; Bacsa, W. S.; Vaugien, Th; Rousset, A. High Specific Surface Area Carbon Nanotubes from Catalytic Chemical Vapor Deposition Process. *Chem. Phys. Lett.* **2000**, *323*, 566–571.
15. Flahaut, E.; Bacsa, R.; Peigney, A.; Laurent, C. Gram-Scale CCVD Synthesis of Double-Walled Carbon Nanotube. *Chem. Commun.* **2003**, 1442–1443.
16. Hiraoka, T.; Kawakubo, T.; Kimura, J.; Taniguchi, R.; Okamoto, A.; Okazaki, T.; Sugai, T.; Ozeki, Y.; Yoshikawa, M.; Shinohara, H. Selective Synthesis of Double-Wall Carbon Nanotubes by CCVD of Acetylene Using Zeolite Supports. *Chem. Phys. Lett.* **2003**, *382*, 679–685.
17. Endo, M.; Muramatsu, H.; Hayashi, T.; Kim, Y. A.; Terrones, M.; Dresselhaus, M. S. Buckypaper from Coaxial Nanotubes. *Nature* **2005**, *433*, 476.
18. Shiozawa, H.; Pichler, T.; Kramberger, C.; Grüneis, A.; Knupfer, M.; Büchner, B.; Zólyomi, V.; Koltai, J; Kürti, J.; Batchlor, D.; *et al*. Fine Tuning the Charge Transfer in Carbon Nanotubes *via* the Interconversion of Encapsulated Molecules. *Phys. Rev. B* **2008**, *77*, 153402−1-4.
19. Shiozawa, H.; Pichler, T.; Kramberger, C.; Rümmeli, M.; Batchlor, D.; Liu, Z.; Suenaga, K.; Kataura, H.; Silva, S. R. P. Screening the Missing Electron: Nanochemistry in Action. *Phys. Rev. Lett.* **2009**, *102*, 046804-1−046804-4.
20. Omata, Y.; Yamagami, Y.; Tadano, K.; Miyake, T.; Saito, S. Nanotube Nanoscience: A Molecular-Dynamics Study. *Phys. E* **2005**, *29*, 454–468.
21. Shibuta, Y.; Maruyama, S. Molecular Dynamics of Generation Process of Double-Walled Carbon Nanotubes from Peapods. *Heat Transfer−Asian Res.* **2006**, *35*, 254–264.
22. Yamaguchi, Y.; Maruyama, S. A Molecular Dynamics Study on the Formation of Metallofullerene. *Euro. Phys. J. D* **1999**, *9*, 385–388.
23. Shibuta, Y.; Maruyama, S. Molecular Dynamics Simulation of Formation Process of Single-Walled Carbon Nanotubes by CCVD Method. *Chem. Phys. Lett.* **2003**, *382*, 381–386.
24. Lindemann, F. A. The Calculation of Molecular Vibration Frequencies. *Phys. Z.* **1910**, *11*, 609–612.
25. Nayak, S. K.; Khanna, S. N.; Rao, B. K.; Jena, P. Thermodynamics of Small Nickel Clusters. *J. Phys.: Condens. Matter* **1998**, *10*, 10853–10862.
26. Tsukada, M. *Computer Program Package TAPP*; University of Tokyo: Tokyo, Japan, 1983−2009.
27. Perdew, J. P.; Burke, K.; Ernzerhof, M. Generalized Gradient Approximation Made Simple. *Phys. Rev. Lett.* **1996**, *77*, 3865–3868.
28. Ding, F.; Rosen, A.; Bolton, K. Molecular Dynamics Study of the Catalyst Particle Size Dependence on Carbon Nanotube Growth. *J. Chem. Phys.* **2004**, *121*, 2775–2779.
29. Raty, J.-Y.; Gygi, F.; Galli, F. Growth of Carbon Nanotubes on Metal Nanoparticles: A Microscopic Mechanism from *ab Initio* Molecular Dynamics Simulations. *Phys. Rev. Lett.* **2005**, *95*, 096103−1-4.
30. Amara, H.; Bichara, C.; Ducastelle, F. Understanding the Nucleation Mechanisms of Carbon Nanotubes in Catalytic Chemical Vapor Deposition. *Phys. Rev. Lett.* **2008**, *100*, 056105−1-4.
31. Zhao, J.; Martinez-Limia, A.; Balbuena, P. B. Understanding Catalyzed Growth of Single-Wall Carbon Nanotubes. *Nanotechnology* **2005**, *16*, S575–S581.
32. Ohta, Y.; Okamoto, Y.; Irle, S.; Morokuma, K. Quantum Chemical Molecular Dynamics Simulation of Single-Walled Carbon Nanotube Cap Nucleation on an Iron Particle. *ACS Nano* **2008**, *2*, 1437–1444.
33. Solovyov, I. A.; Mathew, M.; Solovyov, A. V.; Greiner, W. Liquid Surface Model for Carbon Nanotube Energetics. *Phys. Rev. E* **2008**, *78*, 051601−1-13.
34. Ribas, M. A.; Ding, F.; Balbuena, P. B.; Yakobson, B. I. Nanotube Nucleation *versus* Carbon-Catalyst Adhesion-Probed by Molecular Dynamics Simulations. *J. Chem. Phys.* **2009**, *131*, 224501−1-7.
35. Brenner, D. W. Empirical Potential for Hydrocarbons for Use in Simulating the Chemical Vapor Deposition of Diamond Films. *Phys. Rev. B* **1990**, *42*, 9458–9471.
36. Berendsen, H. J. C.; Postma, J. P. M.; van Gunsteren, W. F.; DiNola, A.; Haak, J. R. Molecular Dynamics with Coupling to an External Bath. *J. Chem. Phys.* **1984**, *81*, 3684–3690.